DALTON
FULL PAPER

Principal component analysis of conformations in fused ring chelate complexes: conformer identification, stereochemistry, and interconversion pathways †

Stephanie E. Harris (née Garner), Isabel Pascual and A. Guy Orpen *

School of Chemistry, University of Bristol, Bristol, UK BS8 1TS

Received 12th April 2001, Accepted 2nd August 2001
First published as an Advance Article on the web 1st October 2001

Data were retrieved from the Cambridge Structural Database for crystal structures containing metal complexes of ethylenediamine (en), tetramethylethylenediamine (tmeda), bis(dimethylphosphino)ethane (dmpe), bis(diphenylphosphino)ethane (dppe) chelate complexes [M(en) (279 structures, 468 fragments), M(tmeda) (156 structures, 181 fragments), M(dmpe) (205 structures, 288 fragments) and M(dppe) (273 structures, 338 fragments)] and *fused* five-membered chelate ring systems [complexes of diethylenetriamine, M(dien) (91 structures, 108 fragments), tris(2-aminoethyl)amine, $M(nn_3)$ (49 structures, 54 fragments), tris(2-diphenylphosphinoethyl)phosphine, $M(pp_3)$, and tris(2-diphenylphosphinoethyl)amine, $M(np_3)$ (54 structures, 56 fragments)], and have been analysed using principal component analysis (PCA) of the intra-ring torsion angles. A limited number of preferred conformers is observed for each system: enantiomeric twist conformations (δ or λ) for M(en), M(tmeda), M(dppe) and M(dmpe); three unique conformers: δδ (and its enantiomer λλ), λδ or δλ for M(dien); and two types for $M(nn_3)$ or $M(xp_3)$ (x = n or p): two enantiomeric C_3 symmetric **A** (λλλ, δδδ) and six equivalent **B** (δλδ, δδλ, λδδ, δλλ, λλδ, and λδλ) conformers of lower symmetry. The pseudorotation pathway for δ ↔ λ interconversion in the single ring systems is clear for M(dppe) and also for M(dmpe) but less so for M(en) and, M(tmeda). The δλ and λδ conformers of M(dien) apparently interconvert through δδ (or λλ) intermediates with one ring at a time inverting. Similarly the interconversion of conformers in the $M(xp_3)$ and $M(nn_3)$ systems seems likely, on the basis of the distribution of structures in conformation space, to follow a sequence δδδ ↔ δλδ ↔ λλδ ↔ λλλ (or its equivalent) but not δδδ ↔ δλδ ↔ δλλ ↔ λλλ. In the M(dien), $M(nn_3)$ and $M(xp_3)$ systems the conformation preferred is linked to the metal coordination geometry. In particular, the presence of an N–M–N angle approaching 180° in a *mer*-octahedral or square-based pyramid stereochemistry in M(dien) species enforces a δλ conformation. Similarly, related *mer*-like stereochemistry in $M(nn_3)$ and $M(xp_3)$ complexes leads to a **B**-type conformation. Longer M–N (or M–P) distances enforce more puckered, symmetrical, twist conformations of five-membered rings. A new pseudo-principal component analysis method is introduced which allows quantitative comparison of conformations in analogous but not identical ring systems. Conformations in M(en) are compared with M(dien) or $M(nn_3)$, with the single-ring system exhibiting less distorted conformations. Phosphine systems exhibit greater variation of conformation than their amine counterparts. In particular M(dmpe) systems show considerably more variation than M(tmeda) whereas M(dppe) species are more varied in conformation than are M(dmpe).

Introduction

The principles of conformational analysis were first applied to co-ordination complexes by Corey and Bailar in 1959.[2] Notably, they found that for metal ethylenediamine complexes [M(en)] there are two energetically and geometrically equivalent enantiomeric conformers, denoted δ and λ (see Fig. 1), which interconvert rapidly at room temperature. They further showed that substituents on M(en) can have either axial or equatorial character, and as for cyclohexane derivatives, bulky substituents prefer equatorial sites. Therefore, M(en) has many of the stereochemical characteristics of cyclopentane and cyclohexane. Gollogly and Hawkins studied mono-, bis- and tris-chelate complexes of en, propylenediamine, and *N*-methylethylenediamine[3] and showed the chelate rings were very flexible, and that a wide range of unsymmetrical *gauche* conformations have similar energy to the C_2 symmetrical δ and λ conformers. There have been further more rigorous molecular mechanics calculations on diamine chelate rings[4] which are in general agreement with the above results, including those by DeHayes and Busch.[5]

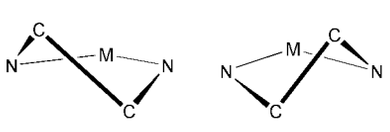

Fig. 1 δ and λ Conformations in five-membered ring chelates.

Concurrent with the molecular mechanics calculations of chelating diamine ligands there have also been numerous NMR studies (see, for example, refs. 6 and 7). However, for M(en) the interconversion is fast on the NMR timescale, and so cannot be easily measured by NMR methods. Goto and co-workers measured the barrier to ring inversion using the paramagnetic complex $[Fe(CN)_4(en)]^-$ (barrier = 24.7 kJ mol^{-1})[8] and Hambley calculated from a strain energy minimization technique a value of 15.7 kJ mol^{-1} for ring inversion in $[Co(en)(NH_3)_4]^{3+}$.[9] Guo *et al.* have recently determined a barrier of 62 kJ mol^{-1} in the solid state for a Pt(en) complex.[10]

Chelate complexes of ethylenediamine and related ligands containing five-membered rings have been very widely used in co-ordination chemistry.[11] Studies of the conformational behaviour of M(en) and other single ring systems based on tetramethylethylenediamine (tmeda), bis(dimethylphosphino)-

† Structural systematics. Part 9.[1]

 DOI: 10.1039/b103297f

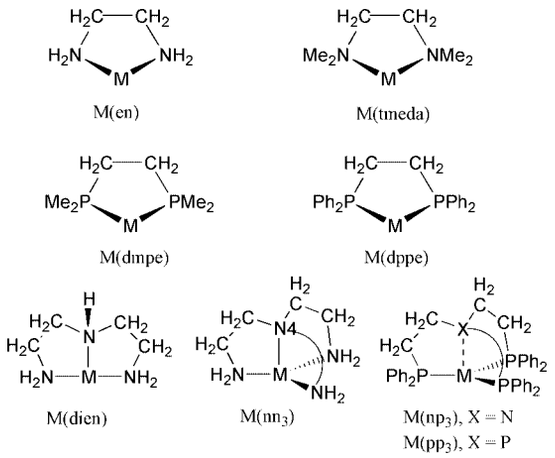

Fig. 2 Sub-molecular fragments analysed; M = Sc–Zn, Y–Cd, La–Hg.

ethane (dmpe), and bis(diphenylphosphino)ethane (dppe) chelate complexes [M(tmeda), M(dmpe) and M(dppe)] are reported in this paper. Related *fused* five-membered ring systems are also analysed as represented by complexes of diethylenetriamine, M(dien), tris(2-aminoethyl)amine, $M(nn_3)$, and the phosphines tris(2-diphenylphosphinoethyl)phosphine, $M(pp_3)$, and tris(2-diphenylphosphinoethyl)amine, $M(np_3)$ (see Fig. 2). These provide a range of archetypal polyamine and polyphosphine complexes containing five-membered rings whose conformational behaviour is of importance in determining their properties. The tridendate ligand dien and the tetradentate ligand nn_3 have found wide use in the chemistry of the transition elements.[11] The related polyphosphine ligands np_3 and pp_3 can be tetradentate or tridentate depending on whether or not there is a central M–X (X = N, P) bond (Fig. 2) and stabilise a variety of metal oxidation states,[12] promoting formation of complexes with highly reactive molecules.[13] Their complexes assume a wide range of co-ordination geometries, including trigonal bipyramidal, square pyramidal, octahedral and tetrahedral, and their reactivity and electronic and geometric structures have been extensively studied, notably by the Florentine school of Sacconi, Bianchini and others.[12–15]

The comparison of different ligating atoms (N and P), different substituents (H, Me Ph) and varying numbers of (fused) chelate rings (1–3) provides information on the contribution that each of these factors makes to the observed conformational behaviour. In this paper we explore the utility of principal component analysis (PCA) as a tool in studying the structural patterns in complex conformational datasets and develop a new derived technique for comparison of similar ring systems in different circumstances. We and others have previously noted the utility of PCA in the study of ring conformations.[16–18] The more familiar Altona and Sundaralingam[19] and Cremer–Pople[20] methods for description of ring conformations have of course been applied to single five-membered ring systems on many occasions, as have other approaches.[17,18,21] PCA in the form used here is a technique for projecting a multi-dimensional dataset so as to present the variation of the parameters optimally, *i.e.* PCA is a method for dimensionality reduction.[22] Since *n*-membered ring conformations have only $(n - 3)$ degrees of freedom[23] one can expect dimensionality reduction to work to at least this extent when applied, for example, to the *n* internal torsion angles of an *n*-membered ring.

The goals of the present work include identification of the favoured conformations in these systems, the pathways for their interconversion, and the links between the conformations adopted and other aspects of the structure of the complexes such as M–L bond lengths and L–M–L bond angles and hence stereochemistry. One aspect of this work has been noted by us in passing[24] and our observations confirmed by others.[25]

Table 1 Number of fragments and structures for the eight sub-molecular targets

Sub-molecular targets	No. of structures	No. of fragments
M(en)	279	468
M(tmeda)	156	181
M(dmpe)	205	288
M(dppe)	273	338
M(dien)	91	108
$M(nn_3)$	49	54
$M(np_3)$, $M(pp_3)$	54	56

Experimental

Data retrieval: crystal structures containing the molecular fragments were located in the Cambridge Structural Database (CSD)[26] (April 1998 version) using the QUEST3D program.[27]

Data analysis: values of bond lengths, bond angles and torsion angles were calculated for each fragment. Principal component analysis and visualisation were carried out with CSD[26,27] and SYSTAT software.[28]

Crystallographic data retrieved were screened manually and automatically and only structures which fulfilled all of the following criteria were retained for further analysis.

(1) Co-ordinates were recorded for the entry.

(2) *R* factor <0.05 for M(en) and M(dppe), <0.07 for M(tmeda) and M(dmpe), <0.08 for M(dien), <0.10 for $M(pp_3)$, $M(np_3)$ and $M(nn_3)$.

(3) No disorder was present in the fragment.

(4) The entry had no errors.

(5) For multiple determinations of the same structure only the 'best' structure as judged by *R* factor and estimated standard deviation of C–C bond lengths was retained.

(6) N–C bonds in the chelate ring(s) were in the range 1.42–1.58 Å, and variation of N–C bonds within a given structure was less than 0.07 Å.

(7) C–C bonds lengths within the chelate ring(s) were in the range 1.44–1.615 Å.

(8) P–C bond lengths were in the range 1.75–1.92 Å.

Original papers were checked as required, especially if the conformation was found to be unusual. These criteria (notably those for bond lengths) are based on initial surveys of bond length distributions and previous studies of ligand dimensions[1,29] and are designed to allow exclusion of disordered structures even in cases where disorder was not explicitly recognised in the original literature.

Table 1 shows the number of fragments used for data analysis and the corresponding number of crystal structures. The endocyclic torsion angles, τ_i $(i = 1, n)$, within the chelate ring(s) were defined as shown in Fig. 3. For those fragments containing phenyl groups, their orientation was defined by recording the C_{ipso}–P–C_{ipso}–C_{orth} torsion angles, ω (see Fig. 4). Eqn. (1) was applied, thereby requiring ω to lie in the range 0–180°.

$$\omega = [(\text{M–P–C–C}') + (\text{M–P–C–C}'') + 180°]/2 \qquad (1)$$

The six ω torsion angles defining the phenyl group orientations in the $M(xp_3)$ fragments are illustrated in Fig. 5. To define the phenyl groups in this way the improper torsion angle P1–X–P3–P2 was required to be positive, so that P1, P2 and P3 are in the clockwise arrangement shown. For each phosphorus atom the torsion angles R_1, R_2 and R_3, illustrated in Fig. 6, were defined $(0 < R < 360°)$ and required to have $R_1 < R_2 < R_3$ (see Fig. 6). Thus R_1 *ca.* 40° is associated with rings A, C and E, *i.e.* ω_1, ω_3 and ω_5, while R_2 *ca.* 160° corresponds to rings B, D and F, *i.e.* ω_2, ω_4 and ω_6.

The torsion angle and bond length and angle datasets were then symmetry expanded according to the conformation space symmetry of the fragment.[23] Principal component analysis was

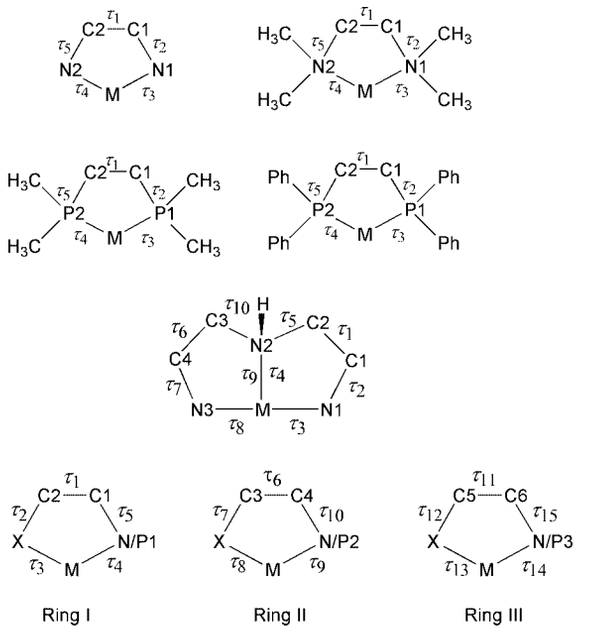

Fig. 3 Definition of torsion angles for M(en), M(tmeda), M(dmpe), M(dppe), M(dien), $M(nn_3)$, and $M(xp_3)$ fragments (X = N or P).

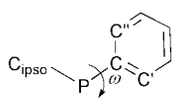

Fig. 4 Definition of torsion angle ω.

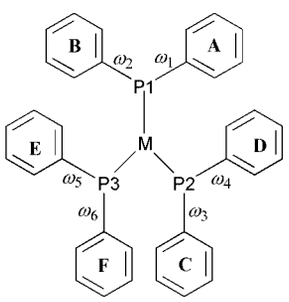

Fig. 5 Definition of ω torsion angles for $M(xp_3)$, as viewed down the X–M bond.

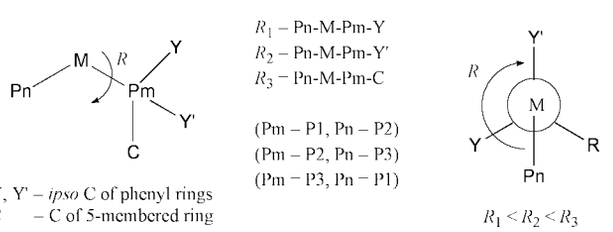

Fig. 6 Definition of torsion angles *R* viewed down the X ··· M vector and the M–Pm bond.

then performed on the expanded τ dataset, and the resulting PCs (principal components) were interpreted by use of scatterplots of the principal component scores, *i.e.* the co-ordinates of each sub-structure in PC-space.[16,30] For the M(en), M(tmeda), M(dmpe) and M(dppe) fragments there are four symmetry equivalent isometric conformations with torsion angles permuted as in Table 2. Therefore, in these cases the symmetry expanded dataset has four times as many sets of torsion angles as there are fragments.

Fig. 3 shows the ten torsion angles which describe the conformation of the M(dien) fragment. The unique hydrogen of the central nitrogen (N2) in the M(dien) fragment was defined as shown in Fig. 3 [H above the $M(N)_3$ plane, and N1 on the right-hand side of the metal] and *S*, the sum of two improper torsion angles is defined as shown in eqn. (2).

Table 2 Symmetry equivalent torsion angle sets for M(en), M(tmeda), M(dmpe) and M(dppe) fragments

E	τ_1	τ_2	τ_3	τ_4	τ_5
σ_{xz}	$-\tau_1$	$-\tau_2$	$-\tau_3$	$-\tau_4$	$-\tau_5$
σ_{yz}	$-\tau_1$	$-\tau_5$	$-\tau_4$	$-\tau_3$	$-\tau_2$
C_2	τ_1	τ_5	τ_4	τ_3	τ_2

$$S = [(\text{N1–N3–N2–C2}) + (\text{N1–N3–N2–C3})] \qquad (2)$$

Therefore, for the configuration as shown in Fig. 3, $S > 0$. The consistent set of data was then symmetry expanded according to its C_S conformation space symmetry yielding two isometric conformations for each fragment with torsion angles as shown in Table 3.

The fragments $M(np_3)$ and $M(pp_3)$ were considered together, defined as $M(xp_3)$, (x = n or p). The $M(xp_3)$ [and $M(nn_3)$] fragments can be considered as three fused five-membered rings, as shown in Fig. 2. The 15 τ torsion angles in the analogous $M(nn_3)$ and $M(xp_3)$ fragments, were defined as shown in Fig. 3.

The unique set of τ values for $M(nn_3)$ and $M(xp_3)$ fragments was then symmetry expanded, as shown in Table 4, according to the conformation space symmetry, here based on the ideal frame group symmetry (C_{3v}) of the MXP_3 or MNN_3 unit. Corresponding permutations of the ω values (see Table 5) and the metal–ligand bond lengths and bond angles were applied.

Finally, the local C_{2v} symmetry of the phenyl groups leads to 180° periodicity in the ω_1 to ω_6 torsions. Therefore the full symmetry group for the $\{\omega, \tau\}$ space is $[(C_2)^2]^3 \wedge C_{3v}$,[31] and there are $[(2)^2]^2 \times 6 = 96$ isometric conformations for each fragment within the 21-dimensional conformation space unit cell which has dimensions 0–360° along each of τ_1 to τ_{15} and ω_1 to ω_6. Six of these lie in the subcell 0–180° in the ω_1 to ω_6 directions.

Principal component analysis

The torsion angle (τ_i) datasets were subjected to principal component analysis (PCA) of the same sort as we and others have previously used.[16–18,32] More strictly, their *z*-scores [$z_j = (\tau_{ij} - \langle\tau_i\rangle)/s_i$, where $\langle\tau_i\rangle$ = mean of τ_i and s_i = standard deviation of τ_i for a given dataset] were subjected to PCA. Such PCA yields eigenvalues of magnitude proportional to the contribution that the corresponding eigenvector makes to the total variance of the standardised dataset. The eigenvectors (or principal components, PCs) produced by PCA are the linear combinations of the original variables (here τ_i) which optimally project their variance in to a new parameter space in which the largest eigenvalue is that for the first principal component (pc1); the next largest is for pc2, and so on.

In order that similar systems could be compared, a new pseudo-PCA technique was developed in which PCA was carried out on the parent five-membered ring system [here M(en)]. Pseudo-PC scores were then derived by first forming pseudo-*z*-scores (pz_j) by dividing the torsion angles for the subject dataset by the standard deviations for the M(en) dataset [$pz_j = (\tau_{ij} - \langle\tau(\text{en})_i\rangle)/s(\text{en})_i$]. Here $\langle\tau_i(\text{en})\rangle = 0$ because of the symmetry expansion. Pseudo-PC scores were then generated by multiplying these pseudo-*z*-scores by the eigenvector matrix obtained for the M(en) dataset. Given the results below (see Table 6) this leads to eqns. (3a)) and (3b)), in which ppc(tw)

$$\text{ppc(tw)} = (0.456\tau_1/51.7) - (0.454\tau_2/39.4) + (0.435\tau_3/14.8) + (0.435\tau_4/14.8) - (0.454\tau_5/39.4) \quad (3a)$$

$$\text{ppc(env)} = (0.203\tau_2/39.4) - (0.677\tau_3/14.8) + (0.677\tau_4/14.8) - (0.203\tau_5/39.4) \quad (3b)$$

Table 3 Symmetry equivalent torsion angle sets for M(dien) fragments

E	τ_1	τ_2	τ_3	τ_4	τ_5	τ_6	τ_7	τ_8	τ_9	τ_{10}
σ	$-\tau_6$	$-\tau_7$	$-\tau_8$	$-\tau_9$	$-\tau_{10}$	$-\tau_1$	$-\tau_2$	$-\tau_3$	$-\tau_4$	$-\tau_5$

Table 4 Symmetry equivalent torsion angle sets for $M(nn_3)$ and $M(xp_3)$ fragments

E	τ_1	τ_2	τ_3	τ_4	τ_5	τ_6	τ_7	τ_8	τ_9	τ_{10}	τ_{11}	τ_{12}	τ_{13}	τ_{14}	τ_{15}
C_3^1	τ_{11}	τ_{12}	τ_{13}	τ_{14}	τ_{15}	τ_1	τ_2	τ_3	τ_4	τ_5	τ_6	τ_7	τ_8	τ_9	τ_{10}
C_3^2	τ_6	τ_7	τ_8	τ_9	τ_{10}	τ_{11}	τ_{12}	τ_{13}	τ_{14}	τ_{15}	τ_1	τ_2	τ_3	τ_4	τ_5
σ_v^1	$-\tau_1$	$-\tau_2$	$-\tau_3$	$-\tau_4$	$-\tau_5$	$-\tau_{11}$	$-\tau_{12}$	$-\tau_{13}$	$-\tau_{14}$	$-\tau_{15}$	$-\tau_6$	$-\tau_7$	$-\tau_8$	$-\tau_9$	$-\tau_{10}$
σ_v^2	$-\tau_{11}$	$-\tau_{12}$	$-\tau_{13}$	$-\tau_{14}$	$-\tau_{15}$	$-\tau_6$	$-\tau_7$	$-\tau_8$	$-\tau_9$	$-\tau_{10}$	$-\tau_1$	$-\tau_2$	$-\tau_3$	$-\tau_4$	$-\tau_5$
σ_v^3	$-\tau_6$	$-\tau_7$	$-\tau_8$	$-\tau_9$	$-\tau_{10}$	$-\tau_1$	$-\tau_2$	$-\tau_3$	$-\tau_4$	$-\tau_5$	$-\tau_{11}$	$-\tau_{12}$	$-\tau_{13}$	$-\tau_{14}$	$-\tau_{15}$

Table 5 Symmetry equivalent torsion angle sets for $M(xp_3)$ fragments

E	ω_1	ω_2	ω_3	ω_4	ω_5	ω_6
C_3^1	ω_5	ω_6	ω_1	ω_2	ω_3	ω_4
C_3^2	ω_3	ω_4	ω_5	ω_6	ω_1	ω_2
σ_v^1	$180 - \omega_2$	$180 - \omega_1$	$180 - \omega_6$	$180 - \omega_5$	$180 - \omega_4$	$180 - \omega_3$
σ_v^2	$180 - \omega_6$	$180 - \omega_5$	$180 - \omega_4$	$180 - \omega_3$	$180 - \omega_2$	$180 - \omega_1$
σ_v^3	$180 - \omega_4$	$180 - \omega_3$	$180 - \omega_2$	$180 - \omega_1$	$180 - \omega_6$	$180 - \omega_5$

Table 6 PCA results for M(en)

Principal component		pc1	pc2
Eigenvalue		4.804	0.195
% Variance explained		96.1	3.9
Torsion angle	Standard deviation (sd)/°[a]	Normalised eigenvectors	
τ_1	51.7	0.456	0.000
τ_2	39.4	−0.454	0.203
τ_3	14.8	0.435	−0.677
τ_4	14.8	0.435	0.677
τ_5	39.4	−0.454	−0.203
Symmetry element		C_2	C_S
Conformation type		Twist	Envelope

[a] Standard deviation of the symmetry expanded torsion angles (°). Owing to symmetry expansion the mean of each of the torsion angles is zero.

is the first PC score describing the degree of C_2 twist in the conformation and ppc(env) the second score, describing the C_s envelope character of the conformation (see below).

Finally, correlations of the principal component scores with other structural parameters were studied and the phenyl group orientations analysed.

Results and discussion

Principal component analysis for M(en)

PCA of the five torsion angles, τ_1 to τ_5, for the four-fold symmetry expanded dataset gave, as expected, two non-zero principal components (PCs). The results of the analysis are shown in Table 6.

Here, pc1 explains 96.1% of the variance in the dataset and its eigenvector describes a twist puckering of the ring with C_2 symmetry; pc2 explains the remaining 3.9% of the variance, and the eigenvector describes an envelope conformation with C_S symmetry. Therefore, pc1 will subsequently be referred to as pc(tw) and pc2 as pc(env).

The scatterplot of pc(tw) against pc(env) scores is shown in Fig. 7(a). The plot has C_{2v} symmetry with four equivalent asymmetric units in which each point represents a particular M(en) fragment. The points cluster around values of pc(tw) *ca.* ±2.2 and zero in pc(env). The centres of these two clusters correspond to symmetrical twist conformations of C_2 symmetry. The points with positive pc(tw) values correspond to δ conformations, whereas for negative pc(tw) values the conformers are of the λ type.

The unpopulated regions with values of pc(env) *ca.* ±1.5 and pc(tw) values close to zero correspond to envelope conformations with C_S symmetry in which the metal is out of the plane of the chelate C_2N_2 moiety (Fig. 8). There is some scatter of points away from pc(env) = 0, leading to structures with asymmetric envelope (or *gauche*) conformations; here, the CH_2 groups are not displaced equally above and below the NMN plane, and both CH_2 groups may be on the same side of the NMN plane (Fig. 8).

Table 7 Torsion angles for M(en) for δ conformers [pc(tw) > 0.0]

Torsion angle	τ_1	τ_2	τ_3	τ_4	τ_5
Mean/°	51.6	−39.1	14.1	14.1	−39.1
Sd/°	3.5	4.2	4.5	4.5	4.2

The observation of only symmetric twist and nearby asymmetric *gauche* conformations but no symmetric envelope forms for M(en) fragments is in agreement with previous studies[2,3] and may be taken to imply that the envelope form has high energy whereas the twist conformer has lower energy. The transition state for interconversion of the δ and λ twist conformers is thought to be an envelope conformation, rather than planar.[3c,8,9] The PC-scatterplot of Fig. 7(a) can be envisaged as mapping part of the pseudorotation pathway[33] for M(en). A similar diagram has been obtained for Co(en) fragments by a statistical treatment and calculation of a potential energy surface by molecular mechanics.[34] PCA of asymmetric furanoside five-membered ring derivatives by Murray-Rust and Motherwell[32] also gave a clustering close to twist conformations. The complete pseudorotation pathway is seen more clearly in the PCA plots of M(dmpe) and M(dppe) fragments (see below and ref. 16).

Table 7 shows the mean values of the torsion angles τ_{1-5} for the δ enantiomer [positive values of pc(tw)], *i.e.* averaging over half of the symmetry expanded data, corresponding to two clusters of points. As a result of the conformation space symmetry, $\langle\tau_2\rangle \equiv \langle\tau_5\rangle$ and $\langle\tau_3\rangle \equiv \langle\tau_4\rangle$, and selection of the

Table 8 PCA results for M(tmeda), M(dmpe) and M(dppe)

	M(tmeda)			M(dmpe)			M(dppe)		
Principal component		pc1	pc2		pc1	pc2		pc1	pc2
Eigenvalue		4.498	0.301		4.295	0.703		3.607	1.392
% Variance explained		93.96	6.02		85.90	14.06		72.14	27.83
Torsion angle	Sd/°	Eigenvector		Sd/°	Eigenvector		Sd/°	Eigenvector	
τ_1	57.2	0.461	0.000	49.7	0.482	0.000	49.5	0.526	0.000
τ_2	40.7	−0.458	−0.215	39.3	−0.475	−0.204	40.1	−0.503	−0.250
τ_3	14.9	0.429	0.674	14.1	0.397	0.677	18.4	0.329	0.661
τ_4	14.9	0.429	−0.674	14.1	0.397	−0.677	18.4	0.329	−0.661
τ_5	40.7	−0.458	0.215	39.3	−0.475	0.204	40.1	−0.503	0.250
Symmetry		C_2	C_S		C_2	C_S		C_2	C_S
Conformation type		Twist	Envelope		Twist	Envelope		Twist	Envelope

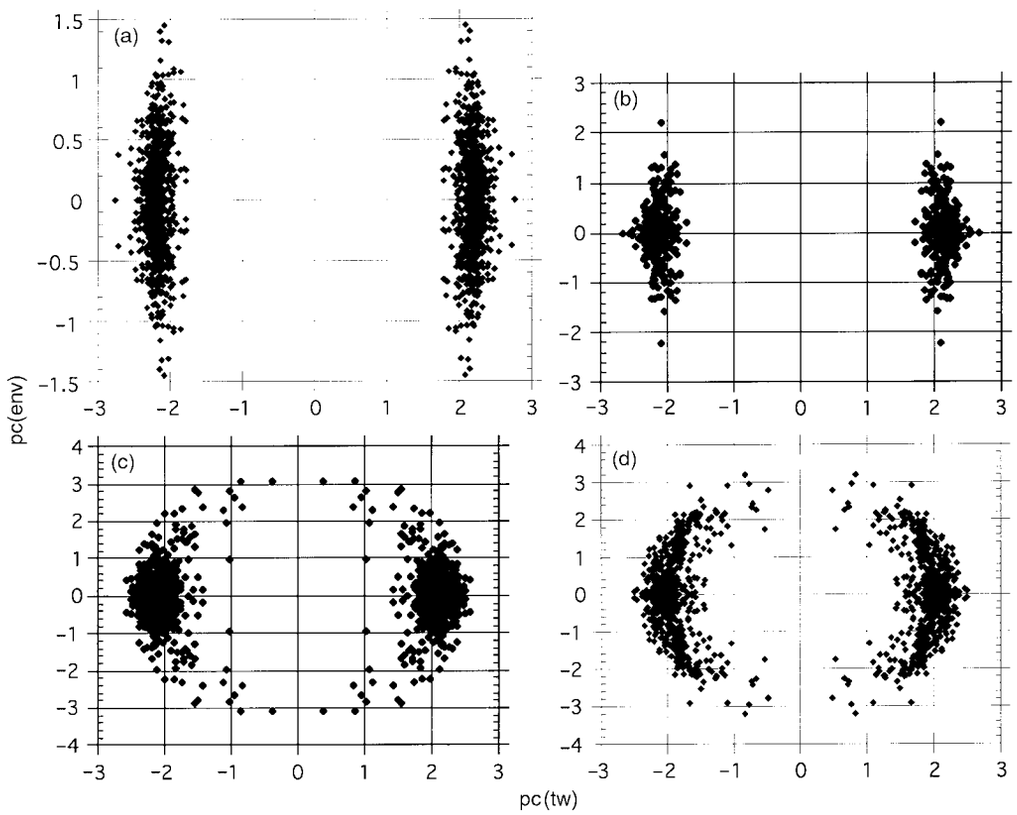

Fig. 7 Scatterplots of pc(tw), pc(env) scores for (a) M(en) fragments, (b) M(tmeda) fragments, (c) M(dmpe) fragments, (d) M(dppe) fragments.

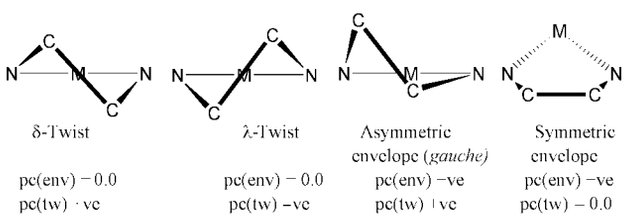

Fig. 8 M(en) conformers.

δ form means that τ_1 is positive. Table 7 shows that τ_1 has the largest torsion angle value, and the smallest standard deviation. This may be taken to imply that the energy requirements of staggering substituents around the C–C bond are paramount. Presumably the much longer M–N bonds mean that non-bonded repulsions between substituents at M and N are reduced relative to those at carbon.[3a,35]

Higher pc(tw) scores correlate significantly, albeit weakly, with the mean M–N distance (Spearman rank correlation coefficient $\rho_s = 0.45$)[36] implying that pure twist conformations are increasingly favoured by chelate rings with long M–N bonds. Beattie and co-workers have suggested that long M–N bonds increase the extent of ring puckering.[3c] There are no other substantial correlations between bond lengths or angles and PC scores.

Principal component analysis of M(tmeda), M(dmpe) and M(dppe)

The results of PCA for the M(tmeda), M(dmpe) and M(dppe) datasets are shown in Table 8. The outcome is broadly similar to that for M(en). Scatterplots of pc(tw) against pc(env) for these systems are shown in Fig. 7(b)–(d).

From Table 8 one can see that pc(tw), (pc1), explains 94% of the variance for M(tmeda) but lesser amounts for M(dmpe) and M(dppe) (86 and 72% respectively). The PCA scores plot for M(tmeda) is also very similar to that for M(en) whereas the M(dmpe) plot [Fig. 7(c)] shows clear evidence of the pseudo-rotation pathway as does that for M(dppe) [Fig. 7(d)] in which the spread within the main cluster of points is most notable. As we have noted for M(dppe) previously,[16] the implication is that the transition state for ring inversion in such five-membered chelates is the C_s envelope conformation. The extension of points from the main clusters towards this conformation is reflected in the percentage of structures lying close to the centre of the clusters of points in each case (see Table 9). The implica-

Table 9 Range of pc(tw) and pc(env) scores for M(en), M(tmeda), M(dmpe) and M(dppe) for the unique sets of fragments with pc(tw) > 0.0 and pc(env) > 0.0

Fragment	Range of pc(tw)	Number (%)[a] 1.8 < pc(tw) < 2.5	Range of pc(env)	Number (%) [a] 0.0 < pc(env) < 0.5
M(en)	1.78–2.76	460/468 (98.2)	0.0–1.45	338/468 (72.2)
M(tmeda)	1.72–2.68	177/181 (97.8)	0.0–2.2	129/181 (71.3)
M(dmpe)	0.38–2.57	254/288 (88.2)	0.0–3.07	163/288 (56.6)
M(dppe)	0.48–2.50	240/338 (71.0)	0.0–3.20	136/338 (40.2)

[a] Number/total and (percentage) of unique fragments in the range specified.

Table 10 Torsion angles for δ conformers of M(tmeda), M(dmpe) and M(dppe)

Fragment	Torsion angle	τ_1	τ_2	τ_3	τ_4	τ_5
M(tmeda)	Mean/°	57.0	−40.3	13.8	13.8	−40.3
	Sd/°	4.6	5.5	5.6	5.6	5.5
M(dmpe)	Mean/°	49.2	−38.4	11.5	11.5	−38.4
	Sd/°	7.2	8.5	8.1	8.1	8.5
M(dppe)	Mean/°	48.8	−37.8	11.3	11.3	−37.8
	Sd/°	8.3	13.3	14.5	14.5	13.3

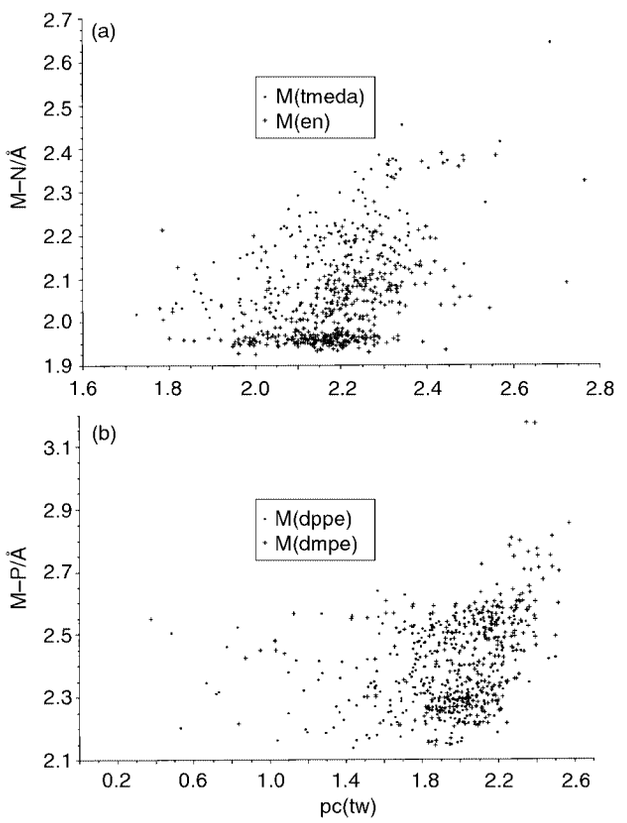

Fig. 9 Scatterplot of (a) M–N and pc(tw) in M(tmeda) and M(en); and of (b) M–P and pc(tw) in M(dmpe) and M(dppe). Values are shown for δ conformers only in each case.

tion is that the barriers to inversion for M(dmpe) and M(dppe) are significantly lower than those for the M(en) and M(tmeda) cases.

The similarity of the M(en) and M(tmeda) plots implies that complexes contributing to these plots have similar potential energy surfaces at least in their lower energy regions. Given that there are few structures with geometries close to the expected envelope transition state for inversion (see below), it is hard to evaluate the relative heights of the barriers to inversion from these plots. The torsion angle means and standard deviations for the δ conformers of the M(tmeda), M(dmpe) and M(dppe) fragments are listed in Table 10. In general, as for M(en), τ_1 has the largest absolute value and the smallest standard deviation.

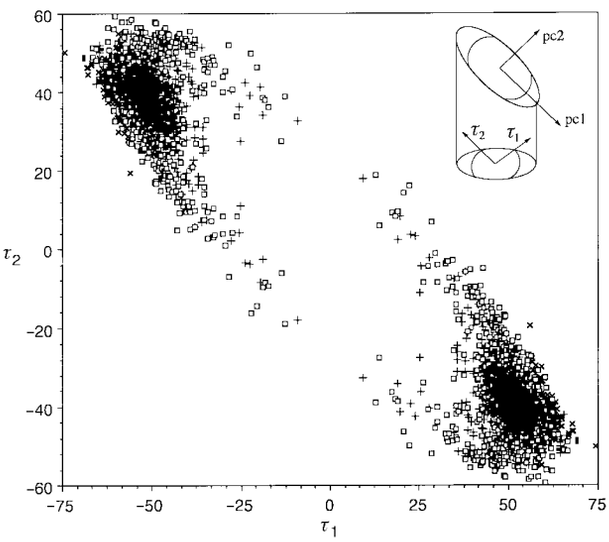

Fig. 10 Scatterplot of τ_1 and τ_2 values for M(en) (■), M(tmeda) (×), M(dmpe) (+) and M(dppe) (□). The inset shows the relationship of PCA and τ_1 *vs.* τ_2 plots.

The slightly larger $\langle\tau_1\rangle$ for M(tmeda) as compared with M(en) might be taken as evidence supporting a generally higher barrier to δ ↔ λ interconversion in tmeda complexes than in M(en) species. In fact, from solution NMR studies, the interconversion barrier from δ to λ for M(tmeda) is of the order of 39 kJ mol^{-1},[37] rather higher than that for M(en) (24.7 kJ mol^{-1}).[8] By the same token, the lower values of $\langle\tau_1\rangle$ for M(dmpe) and M(dppe) are in accord with the suggestion made above that the barriers are lower in these cases. These lower barriers presumably result from the effects of the longer bond lengths in the diphosphine chelate rings and the reduced steric interactions that result.

It is notable that the values of τ_3 and τ_4 are relatively small compared with τ_1, τ_2 and τ_5 implying that the rings are flatter in the region near the metal, for reasons related to those noted for M(en) above. Weak but statistically significant correlations between M–L bond distances and pc1 scores are again evident [see Fig. 9; Spearman rank correlation coefficients 0.65, 0.45, 0.24 for M(tmeda), M(dmpe) and M(dppe) respectively].

Hambley[9] obtained a potential energy surface for $[Co(en)(NH_3)_4]^{3+}$ by minimising the strain energy of the Co(en) chelate ring as a function of τ_1 and τ_2. Fig. 10 shows a scatterplot of τ_1 *versus* τ_2 for the symmetry expanded datasets for M(en), M(tmeda), M(dmpe) and M(dppe) fragments combined. The distribution of points in Fig. 10 is very similar to the low energy regions of Hambley's potential energy surface and thus this also maps the pseudorotation pathway from δ to λ conformations. The cluster of points with positive τ_1 represents δ conformations and those with negative τ_1 correspond to the λ conformers. The points linking the two clusters extend towards C_s envelope conformations (τ_1 near zero). As noted above these data points are primarily from the M(dppe) and M(dmpe) fragments.

Fig. 10 also illustrates the relationship between the PC axes and the projection on to the τ_1 and τ_2 axes. The projection of the

Table 11 PCA results for M(dien)

Principal component			pc1	pc2	pc3	pc4
Eigenvalue			6.351	2.564	0.811	0.269
% Variance explained			63.5	25.6	8.11	2.69
Torsion angle	Mean/°	Sd/°	Normalised eigenvectors			
τ_1	29.125	41.6	0.344	0.304	0.012	0.175
τ_2	−19.558	27.9	−0.317	−0.362	−0.173	−0.023
τ_3	4.606	9.5	0.152	0.445	0.603	−0.435
τ_4	11.341	17.8	0.359	0.141	−0.306	0.446
τ_5	−24.648	36.1	−0.359	−0.241	0.113	−0.285
τ_6	29.125	41.6	−0.344	0.304	−0.012	0.175
τ_7	19.558	27.9	0.317	−0.362	0.173	−0.023
τ_8	−4.606	9.5	−0.152	0.445	−0.603	−0.435
τ_9	−11.341	17.8	−0.359	0.141	0.306	0.446
τ_{10}	24.648	36.1	0.359	−0.241	−0.113	−0.285
Symmetry element			C_s	C_2	C_s	C_2
Conformation type[a]			Twist	Twist	Envelope	Twist

[a] Conformation of the individual five-membered rings.

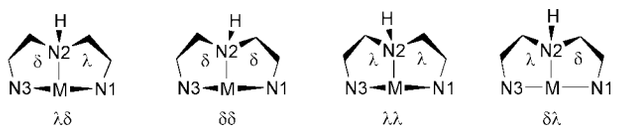

Fig. 11 M(dien) conformers.

dataset on to axes τ_1 and τ_2, while helpful, is not optimal and conceals much of the overall variation within the dataset. In contrast, projection on to {pc1, pc2} is optimal and shows 100% of the variation in the dataset because there are only two degrees of freedom required to describe the conformations of a five-membered ring.[23]

Principal component analysis of M(dien)

Diethylenetriamine is a tridentate ligand in whose complexes the conformation of the two five-membered rings can be described as δ or λ. There are, therefore, four possible conformer types: δδ, λλ, δλ and λδ. The δδ and λλ forms are asymmetric enantiomers whereas the diastereomeric δλ and λδ each have C_s symmetry with the mirror plane through the central nitrogen (N2).[38] The four conformers are shown in Fig. 11.

If PCA is to be successful for the M(dien) case one would not only expect a reduction in the conformation space dimensionality (to four or less given the two dimensions required for each five-membered ring), but also for the analysis to distinguish the four possible conformers as well defined clusters of conformations in the scatterplot. In practice, PCA of the ten torsion angles of the M(dien) fragment for the two-fold symmetry expanded dataset, gave four non-zero principal components. The results of this analysis are shown in Table 11. Pc4 explains only 2.7% of the variance and has not been analysed further. The choice of how many principal components to analyse in depth in this paper is dictated by the practical need to be able to visualise the variation in the torsion angle dataset. It seems unlikely that highly (chemically) significant aspects of conformational behaviour will be lost by this approach given the relatively small percentage variance described by the PCS not analysed further.

PCA has been successful in reducing the dimensionality of this fused ring system from ten to four, and 89% of the variance can be explained by only two PCs. Reduction to four PCs is as one would expect for a system with two five-membered rings, as noted above. The pc1 eigenvector has C_s symmetry, and from the τ_1 and τ_6 values (τ_1 = +ve, τ_6 = −ve), it describes a δλ type conformation for positive values of pc1, and a λδ conformation for highly negative values. This eigenvector describes an asymmetric envelope conformation for the two five-membered rings since for each ring it is similar in form but not identical to the eigenvector of pc1 of M(en). Pc2 has C_2 symmetry, and implies a δδ type conformation for positive scores and λλ conformation for negative scores with the five-membered rings in asymmetric envelope conformations. Pc3 has C_s symmetry and is similar in form to pc2 of M(en), describing envelope conformations of the two five-membered rings.

Fig. 12(a) shows a scatterplot of the pc1 and pc2 scores. The M(dien) fragments lie in four distinct clusters corresponding to the four conformers, δδ, λλ, δλ and λδ. The two clusters at extreme values of pc1 and zero in pc2 are the δλ and λδ conformers, whereas the clusters at extreme values of pc2 and *ca.* −2 in pc1 are the δδ and λλ conformers. There are 74 unique fragments in the δλ cluster, 18 in each of the δδ and λλ clusters, and 16 unique fragments in the λδ cluster. The distribution of points in Fig. 12(a) has mirror symmetry, which mirror relates the enantiomeric δδ and λλ clusters, and bisects the diastereomeric δλ and λδ conformers. The plot of pc1 and pc3 scores is shown in Fig. 12(b). The scatterplot illustrates that there is substantial variation in the conformations of the δδ and λλ and, to a lesser extent, δλ conformers along the pc3 direction.

It is clear that in this case PCA has been successful in reducing the dimensionality and thus the number of parameters needed to define the conformations of the M(dien) fragment, and it has also successfully divided the 108 fragments into the four conformational types. The mean torsion angles for the δλ, δδ and λδ conformers are given in Table 12. The δδ (and λλ) conformations show the largest variations (*i.e.* largest standard deviations), and thus appear to be the most flexible [as implied by Fig. 12(b)]. The interconversion of δλ and λδ conformers seems likely to proceed through δδ (or λλ) intermediates with one ring at a time inverting, presumably by a pseudorotation mechanism.

A plot of pc1 scores against N1MN3 bond angles for the structures of a unique set of conformers, *i.e.* for those with positive pc2 scores, is shown in Fig. 12(c). The plot clearly shows the division of the *fac* and *mer* isomers, and that there is a difference in the N1MN3 bond angle range for the δδ (or λλ) and λδ conformers. The points corresponding to the λδ conformers have an N1MN3 angle close to 90° whereas the δδ conformers show a much larger range of N1MN3 angles, from 90 to 140°. The implication is that the δδ (and λλ) conformers are able to accommodate a wider range of metal coordination geometries, including those between *fac* and *mer*. Finally, all the structures with N1–M–N3 angles over 150° have δλ conformations. These observations imply that the conversion of λδ conformers to δλ requires the assistance of geometry variation at the metal.

The dependence of the conformation of M(dien) upon the coordination geometry at M was discussed by Schmidtke

Table 12 Mean torsion angles (and their standard deviations) for δλ, δδ and λδ conformers of M(dien) fragments

Conformer	Torsion angle	τ_1	τ_2	τ_3	τ_4	τ_5	τ_6	τ_7	τ_8	τ_9	τ_{10}
δλ	Mean/°	52.0	−33.2	6.2	22.3	−45.9	−52.0	33.2	−6.2	−22.3	45.9
	Sd/°	4.3	5.0	4.5	4.2	4.3	4.3	5.0	4.5	4.2	4.3
δδ	Mean/°	50.0	−45.1	22.8	3.8	−29.6	49.6	−31.5	6.6	19.7	−42.1
	Sd/°	6.2	5.2	7.0	8.4	8.9	5.9	11.3	10.9	8.6	5.1
λδ	Mean/°	−44.2	29.0	−6.7	−17.5	38.8	44.2	−29.0	6.7	17.5	−38.8
	Sd/°	2.4	5.0	5.5	5.0	4.3	2.4	5.0	5.5	5.0	4.3

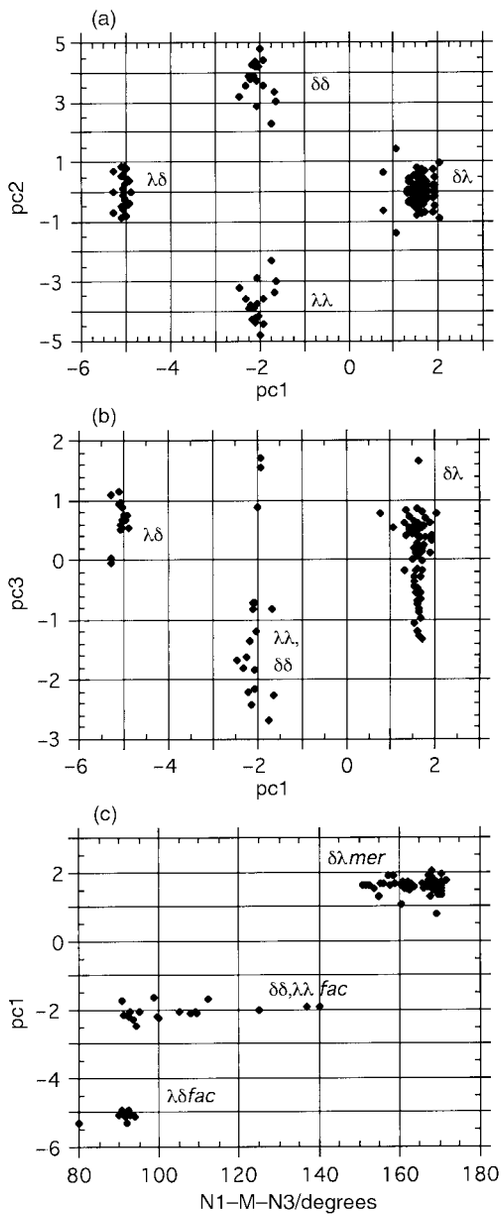

Fig. 12 Scatterplot of (a) pc1 and pc2 scores for M(dien) fragments, (b) pc1 and pc3 scores for M(dien) fragments, and (c) plot of pc1 score *vs.* N1–M–N3 angle for M(dien).

and Garthoff in the late 1960s, based on IR spectroscopic evidence.[38] They suggested that for the *mer* isomer only the δλ conformer is possible, where the other conformers are sterically unfavourable. For the *fac* co-ordination the most likely form was said to be δδ or λλ. The λδ conformer was "ruled out because of the steric hindrance due to hydrogen atoms". Molecular mechanics studies[39] have been performed on $[Co(dien)_2]^{2/3+}$ and for the *mer* isomer the (δλ,δλ) conformer was found to be of the lowest energy. Molecular mechanics calculations for *u-fac*-$[Co(dien)_2]$ conformers gave (λδ,λδ) as the most stable form, for Co(III), and the (λλ,λλ) form for Co(II). The energy difference between the conformers was found to

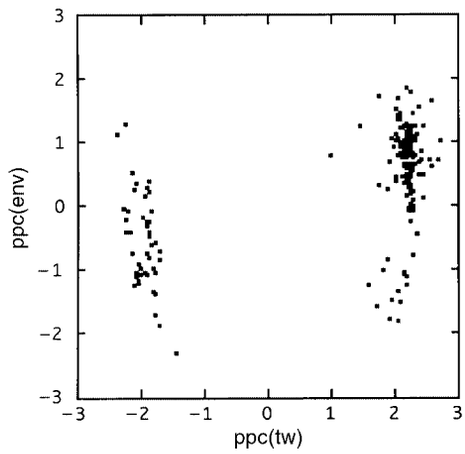

Fig. 13 Scatterplot of pseudo-PCA scores for M(dien) fragments.

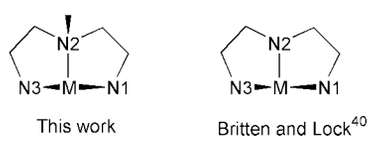

Fig. 14 Alternative conventions for *fac* isomers of M(dien).

be relatively small. A recent report on conformations and configurations of $[Ni(dien)_2]^{2+}$ including DFT calculations reached analogous conclusions.[25] These calculations therefore are in accord with our conclusions as presented above.

Comparison of M(dien) with M(en)—use of pseudo-PCA

Pseudo-PC scores, ppc(tw) and ppc(env), were calculated for τ_{1-5} of the symmetry expanded dataset of M(dien), and the corresponding scores plot is shown in Fig. 13. Most of the five-membered rings of M(dien) have an asymmetric envelope conformation with ppc(env) *ca.* ±1, with only a few conformations close to a pure C_2 twist conformation [ppc(env) ≈ 0.0]. The plot has no symmetry and does not come close to resembling the C_{2v} symmetry of the M(en) plot [Fig. 7(a)]. 78 of 109 (72.0%) data points lie in the range ppc(tw) = 1.8 to 2.5, and −1.8 to −2.5, and 29 of 108 (26.9%) points in the range ppc(env) = −0.5 to +0.5. Both of these percentages are lower than for the single five-membered rings of M(en) and M(tmeda) (see Table 9 and Figs. 7 and 8), implying that the five-membered rings adopt more asymmetric (and presumably strained) conformations in M(dien) fragments. The fragment shows limited variability of conformation, as there are large empty regions of conformation space between the four clusters in Fig. 19, and thus it is not possible to identify the pathways linking them in detail. This is consistent with the limited flexibility of the five-membered rings in M(en) and M(tmeda) fragments noted above.

Britten and Lock in their discussion of M(dien) conformations have used a different convention[40] in which the metal atom is placed behind the plane of the three nitrogen atoms with N1 to the right of the metal. This results in rings assigned in the opposite sense to our definition (see Fig. 14). Comparison of the conformer assignments given by Britten and Lock for

Table 13 Comparison of conformer assignments for M(dien) structures

Compound	Refcode	Isomer	Britten and Lock conformer type[a]	PCA conformer type[b]
$[Mo(dien)O_3]$	ODEAMO	*fac*	δλ	λδ
$[\pi\text{-}Co(en)(dien)Cl]^{2+}$	KENCTO	*fac*	δλ	λδ
$[\omega\text{-}Co(en)(dien)Cl]^{2+}$	ENCOCL01	*fac*	δλ	λδ
$[Pt(dien)Cl_3]^+$	ENTAPT	*fac*	λλ	λλ
$[Pt(dien)NO_3]NO_3$	BAGLAW10	*mer*	δλ	δλ
[Pt(dien)Br]Br	BDETAP	*mer*	δλ	δλ
[Pt(dien)Cl]Cl	BIFBAT	*mer*	λδ	δλ
$[Pt(dien)Br]_2PtBr_4$ A	ETRPTB	*mer*	δλ	δλ
$[Pt(dien)Br]_2PtBr_4$ B	ETRPTB	*mer*	δλ	δλ
$[Pt(dien)Guo](NO_3)_2$	TGUOPT	*mer*	λδ	δλ

[a] From ref. 40. [b] From this study.

Table 14 Results of PCA for $M(nn_3)$ fragments

Principal component		pc1	pc2	pc3	pc4	pc5	pc6
Eigenvalue		5.316	3.815	3.815	0.799	0.799	0.453
% Variance explained		35.3	25.4	25.4	5.3	5.3	3.0
Torsion angle	Sd/°	Normalised eigenvectors					
τ_1	46.7	0.268	0.268	0.292	0.014	0.123	0.090
τ_2	38.8	−0.198	−0.302	−0.329	0.006	0.057	−0.167
τ_3	19.6	0.071	0.311	0.340	−0.038	−0.339	0.266
τ_4	15.3	0.338	0.033	0.036	0.072	0.647	−0.210
τ_5	33.6	−0.321	−0.209	−0.228	−0.036	−0.327	0.015
τ_6	46.7	0.268	−0.387	0.086	0.099	−0.073	0.090
τ_7	38.8	−0.198	0.436	−0.097	0.046	−0.034	−0.167
τ_8	19.6	0.071	−0.450	0.100	−0.274	0.202	0.266
τ_9	15.3	0.338	−0.048	0.011	0.524	−0.386	−0.210
τ_{10}	33.6	−0.321	0.302	−0.067	−0.265	0.195	0.015
τ_{11}	46.7	0.268	0.119	−0.378	−0.113	−0.050	0.090
τ_{12}	38.8	−0.198	−0.134	0.426	−0.053	−0.023	−0.167
τ_{13}	19.6	0.071	0.139	−0.439	0.312	0.137	0.266
τ_{14}	15.3	0.338	0.015	−0.046	−0.596	−0.261	−0.210
τ_{15}	33.6	−0.321	−0.093	0.295	0.302	0.132	0.015
Symmetry element		C_3	—	—	—	—	C_3
Conformation type[a]		Twist	Twist	Twist	Envelope	Envelope	—

[a] Conformation of the individual five-membered rings.

particular structures with ours shows a number of discrepancies as listed in Table 13. For *fac* isomers the reversal of rings explains the apparent difference. However, four of the *mer* structures were assigned by Britten and Lock as having δλ conformations (as opposed to λδ, as they should have been). Apparently this is because for *mer* structures it is problematic to assign the metal position relative to the N_3 plane since it lies very close to that plane.

Principal component analysis of $M(nn_3)$ fragments

$M(nn_3)$ complexes of tris(2-aminoethyl)amine contain three five-membered rings fused together with all three rings sharing the central M–N4 bond (see Fig. 2). All the structures contain tetradentate nn_3 ligands. Principal component analysis of the 15 torsion angles of the symmetry expanded dataset gave, as expected, six non-zero PCs shown in Table 14.

Pc1 explains 35.3% of the variance and positive values describe a twist conformation for each of the five-membered rings and a C_3 symmetric δδδ conformation. Pc2 and pc3 are symmetry degenerate, each explaining 25.4% of the variance and do not possess C_3 symmetry, but describe distorted δλδ and δδλ conformations respectively. Pc4 and pc5 are also symmetry degenerate, these eigenvectors describing distorted envelope conformations of the five-membered rings. As these two PCs of $M(nn_3)$ each explain only 5.3% of the variance, they will not be considered further; the analysis will be confined to the first three PCs which explain 86.1% of the total variance.

Fig. 15(a) shows pc1 against pc2 scores for the expanded dataset for $M(nn_3)$; Fig. 15(b) (left) shows the plot of pc2 scores against pc3 scores and has C_{3v} symmetry. Fig. 15(b) (right) indicates schematically the locations of the eight clusters of points that may be identified in the (pc1, pc2, pc3) space. Clusters **A** and **A′** have large pc1 scores (*ca.* ±4.0), and pc2 (and pc3) scores close to zero and have C_3 symmetric δδδ conformations for positive pc1 scores and λλλ conformations for negative values (see Fig. 16). The six remaining clusters are equivalent and are denoted as **B** (positive pc1 scores) and **B′** (negative pc1 scores) with δλδ (**B**^{1}), δδλ (**B**^{2}), λδδ (**B**^{3}),δλλ (**B′**^{1}), λλδ (**B′**^{2}), and λδλ (**B′**^{3}) conformations respectively (see Fig. 16). Sargeson *et al.* have carried out strain-energy minimisation calculations on the octahedral cation $[Co(nn_3)(en)]^{3+}$, which showed that the enantiomorphic conformations of type **B** and **B′** observed in our analysis were the most energetically stable, by 11.3 kJ mol^{-1} compared with the next set.[41] They observed that in trigonal bipyramidal (tbp), five-co-ordinate complexes the $M(nn_3)$ fragment typically adopts a λλλ (or δδδ) conformation, although no strain-energy calculations were carried out. The mean torsion angles for δδδ and δλδ conformations are given in Table 15 (see Fig. 16) and are discussed below in comparison with those for $M(xp_3)$ fragments.

Comparison of $M(nn_3)$ with M(en)—use of pseudo-PCA

Pseudo-PC scores, ppc(tw) and ppc(env), were calculated for τ_{1-5} of the symmetry expanded dataset of $M(nn_3)$ (see Fig. 17). Most of the five-membered rings of $M(nn_3)$ have an asymmetric envelope conformation with ppc(env) between ±1 and ±2, with only a few conformations close to a twist conformation [ppc(env) ≈ 0.0]. Although the plot only has inversion

Table 15 Mean torsion angles for δδδ (**A**) and δλδ (**B**[1]) conformers of $M(nn_3)$ fragments

δδδ Conformers. Mean torsion angles (sd)/°; 14 fragments				
τ_1, τ_6, τ_{11}	τ_2, τ_7, τ_{12}	τ_3, τ_8, τ_{13}	τ_4, τ_9, τ_{14}	τ_5, τ_{10}, τ_{15}
51.5 (3.3)	−35.4 (4.9)	10.4 (6.4)	16.3 (7.2)	−40.3 (7.3)
δλδ Conformers. Mean torsion angles (sd)/°; 40 fragments				
τ_1	τ_2	τ_3	τ_4	τ_5
40.3 (4.1)	−20.6 (2.6)	−1.4 (2.8)	23.5 (4.0)	−40.4 (5.1)
τ_6	τ_7	τ_8	τ_9	τ_{10}
−45.0 (2.8)	47.5 (2.0)	−28.4 (1.7)	4.8 (2.0)	20.1 (2.4)
τ_{11}	τ_{12}	τ_{13}	τ_{14}	τ_{15}
48.5 (4.2)	−45.4 (1.7)	23.9 (3.0)	1.6 (4.5)	−27.0 (5.3)

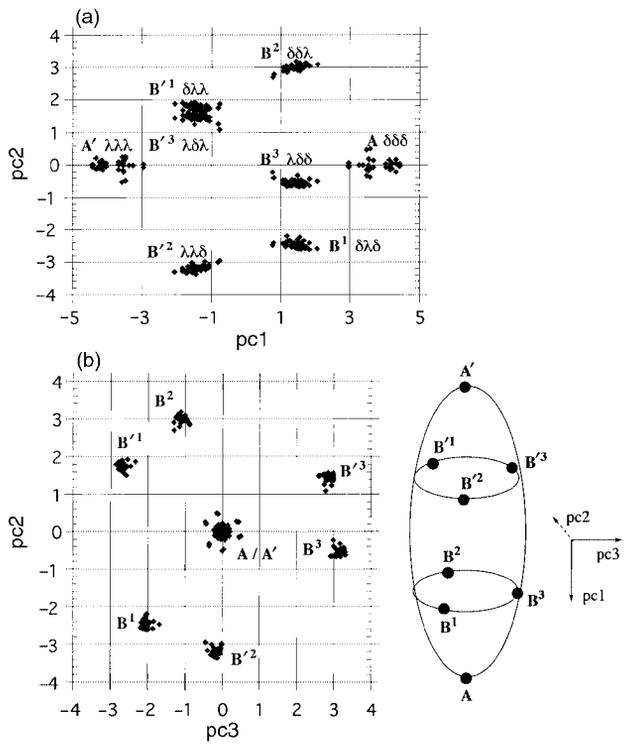

Fig. 15 (a) Scatterplot of pc1 and pc2 scores for $M(nn_3)$ fragments; (b) (left) scatterplot of pc2 and pc3 scores for $M(nn_3)$ fragments, and (right) schematic location of clusters **A** and **B** in the (pc1, pc2, pc3) space.

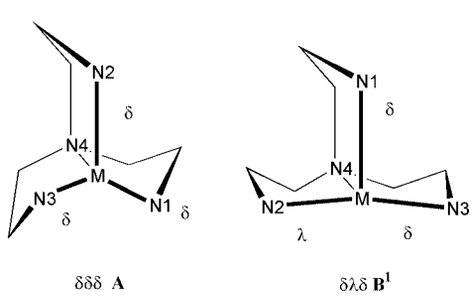

Fig. 16 **A** (δδδ) and **B**[1] (δλδ) conformers of $M(nn_3)$.

symmetry the points are nearly equally distributed either side of zero in ppc(env). Considering only the rings with δ conformations, 116 of 162 (71.6%) ring conformations lie in the range ppc(tw) = 1.8–2.5, and 26 of 162 (16.0%) lie in the range ppc(env) = −0.5 to +0.5. Both of these percentages are lower than for the single five-membered rings of M(en) and M(tmeda) (see Table 9 and Figs. 7 and 8) implying that the five-membered rings in $M(nn_3)$ structures adopt somewhat strained and asymmetric conformations.

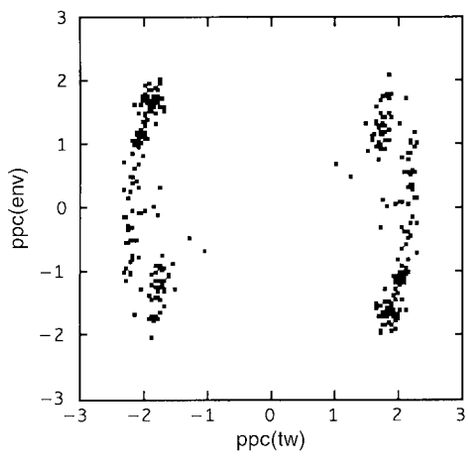

Fig. 17 Pseudo-principal component scatterplot for MN_2C_2 fragments of $M(nn_3)$.

$M(pp_3)$ and $M(np_3)$ conformations

The fragments $M(pp_3)$ and $M(np_3)$ are composed of three five-membered rings fused so that all three rings share the M···X (X = P [$M(pp_3)$] or N [$M(np_3)$]) vector and the ligand can either be tetradentate or tridentate. Of the 56 $M(xp_3)$ fragments obtained, 34 are $M(np_3)$ and the remaining 22 $M(pp_3)$. PCA of the 15 torsion angles of the C_{3v} symmetry expanded data gave six non-zero PCs shown in Table 16.

In terms of the individual five-membered rings, torsion angles τ_1, τ_6 and τ_{11} for rings I, II and III of $M(xp_3)$ are equivalent to τ_1 for M(en), as shown in Fig. 3. Although the amounts of variation explained by pc1–3 are rather different the forms of these components are equivalent to those for the $M(nn_3)$ fragment. The symmetry degenerate pair pc2, pc3 have apparently different form, but misleadingly so since their form is arbitrary in the sense that there are infinite varieties of linear combinations that may be taken to form such degenerate components.[17] Similar observations hold for the less significant PCs for these two datasets. Thus the degenerate pair pc5 and pc6 for the $M(xp_3)$ dataset are equivalent to pc4 and pc5 for $M(nn_3)$, and the C_3 symmetric pc4 for the $M(xp_3)$ dataset is equivalent to pc6 for $M(nn_3)$.

The clusters of conformations seen in Figs. 18(a) and (b) are similar to those for the $M(nn_3)$ fragment, there being eight distinct clusters of conformations of type **A**, **A**′, **B** and **B**′. While the conformer types are the same the clusters appear to be more diffuse and offer some insight into the interconversion of conformers. Thus it appears that the likely least-motion route for conversion of a δδδ conformer to λλλ involves one five-membered ring at a time flipping from δ to λ conformation. The overall process is therefore δδδ ↔ δλδ ↔ λλδ ↔ λλλ (or its equivalents δδδ ↔ δδλ ↔ δλλ ↔ λλλ and δδδ ↔ λδδ ↔ λδλ ↔ λλλ). It seems likely that other conceivable one-ring-a-time pathways are less favoured (*e.g.* δδδ ↔ δλδ ↔ δλλ ↔ λλλ)

Table 16 PCA results for $M(xp_3)$

Principal component		pc1	pc2	pc3	pc4	pc5	pc6
Eigenvalue		10.66	1.268	1.268	1.262	0.261	0.261
% Variation explained		71.1	8.5	8.5	8.4	1.7	1.7
Torsion angle	Sd/°	Normalised eigenvectors					
τ_1	51.6	0.278	0.054	0.360	0.005	−0.060	0.003
τ_2	38.2	−0.266	−0.062	−0.413	0.129	−0.022	0.001
τ_3	12.7	0.198	0.068	0.450	−0.445	0.263	−0.012
τ_4	16.1	0.262	0.032	0.215	0.316	−0.284	0.013
τ_5	41.7	−0.278	−0.048	−0.320	−0.137	0.139	−0.006
τ_6	51.6	0.278	0.285	−0.227	0.005	0.028	−0.054
τ_7	38.2	−0.266	−0.327	0.260	0.129	0.010	−0.019
τ_8	12.7	0.198	0.356	−0.284	−0.445	−0.121	0.234
τ_9	16.1	0.262	0.170	−0.136	0.316	0.131	−0.252
τ_{10}	41.7	−0.278	−0.253	0.202	−0.137	−0.064	0.124
τ_{11}	51.6	0.278	−0.339	−0.133	0.005	0.033	0.051
τ_{12}	38.2	−0.266	0.389	0.153	0.129	0.012	0.018
τ_{13}	12.7	0.198	−0.424	−0.167	−0.445	−0.142	−0.222
τ_{14}	16.1	0.262	−0.203	−0.080	0.316	0.153	0.240
τ_{15}	41.7	−0.278	0.302	0.119	−0.137	−0.075	−0.118
Symmetry element		C_3	—	—	C_3	—	—
Conformation type[a]		Twist	Twist	Twist	Envelope	—	—

[a] Conformation of the individual five-membered rings.

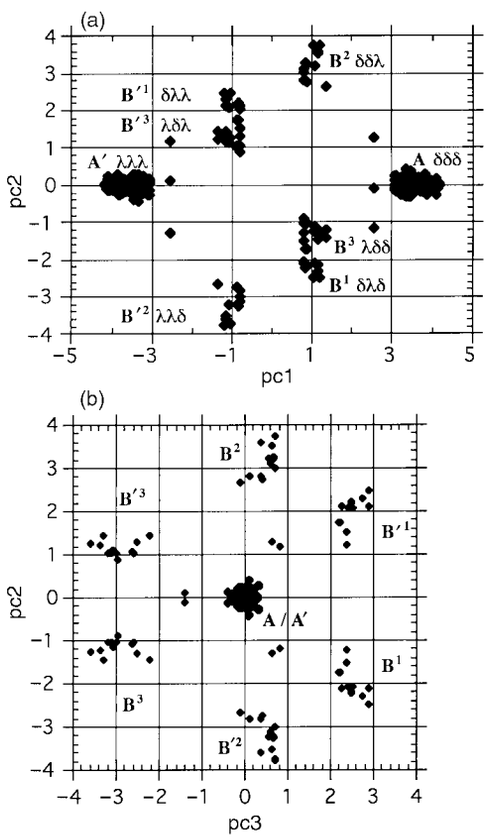

Fig. 18 Scatterplot of (a) pc1 and pc2 scores for $M(xp_3)$ fragments, and (b) pc2 and pc3 scores for $M(xp_3)$ fragments.

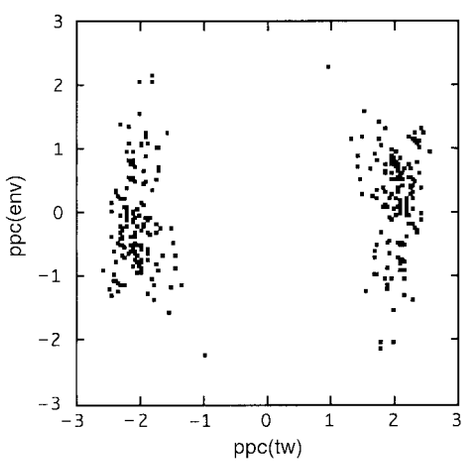

Fig. 19 Pseudo-principal component plot for $MXPC_2$ fragments of $M(xp_3)$ (X = N or P).

given that the $\mathbf{B}^1$ (δλδ) cluster is much closer to the $\mathbf{B}'^2$ (λλδ) cluster than the $\mathbf{B}'^1$ (δλλ) (see Fig. 15). This proximity effect is directly related to the coordination geometry at the metal (see below).

The mean torsion angles for the **A** (δδδ) and the $\mathbf{B}^1$ (δλδ) conformers are given in Table 17. While the mean values are similar to those for $M(nn_3)$ the standard deviations are generally higher than for $M(nn_3)$. This is in accord with an earlier observation for single ring systems, where the amine derivatives showed less flexibility than their phosphine analogues. Pseudo-PC scores, ppc(tw) and ppc(env), were calculated for τ_1 to τ_5 of the symmetry expanded data of $M(xp_3)$. Fig. 19 shows the scatterplot of pseudo-PC scores for five-membered rings of the $M(xp_3)$ dataset. Considering only the δ conformations [ppc(tw) > 0] there is a slight preference for positive values of ppc(env), which corresponds to the CH_2 group bonded to PPh_2 being further out of the XMP plane than the other methylene in an asymmetric envelope conformation. For δ conformers where ppc(env) is negative the CH_2 group bonded to X is the further out of plane. There are also a number of points with a ppc(env) score of *ca.* 0.0, corresponding to a symmetrical twist conformation. The distribution of points is not as asymmetric as for M(dien) (see Fig. 13) or $M(nn_3)$ (see Fig. 17). 141 of 168 (83.9%) fragments in the δ cluster lie in the range of ppc(tw) = 1.8–2.5, and 68 of 168 (40.5%) lie in the range pc(env) = −0.5 to 0.5. These percentages are lower than for the single five-membered rings of M(en) and M(tmeda), similar to those of M(dmpe) and M(dppe) (see Table 9 and Figs. 7 and 8), and somewhat above those for M(dien) and $M(nn_3)$ implying that the five-membered rings in $M(np_3)$ structures are not significantly more distorted or strained than in the single ring diphosphine case. This is in contrast to the situation for M(dien) and $M(nn_3)$ for which the constraints of multiple ring formation lead to greater distortions than for the corresponding single ring diamine systems.

Table 17 Mean torsion angles for the δδδ (**A**) and the δλδ (**B**[1]) conformers of $M(xp_3)$ fragments

δδδ Conformers. Mean torsion angles (sd)/°; 43 fragments				
τ_1, τ_6, τ_{11}	τ_2, τ_7, τ_{12}	τ_3, τ_8, τ_{13}	τ_4, τ_9, τ_{14}	τ_5, τ_{10}, τ_{15}
52.5 (7.2)	−37.9 (6.4)	9.8 (7.2)	14.8 (7.4)	−41.8 (10.3)

δλδ Conformers. Mean torsion angles (sd)/°; 13 fragments				
τ_1	τ_2	τ_3	τ_4	τ_5
41.2 (6.9)	−24.3 (5.8)	−0.1 (4.1)	19.2 (3.5)	−38.4 (4.2)
τ_6	τ_7	τ_8	τ_9	τ_{10}
−47.7 (4.0)	43.7 (8.7)	−18.2 (8.4)	−5.7 (6.8)	32.3 (6.4)
τ_{11}	τ_{12}	τ_{13}	τ_{14}	τ_{15}
49.0 (5.4)	−39.5 (6.5)	12.6 (5.4)	11.7 (4.1)	−37.5 (3.9)

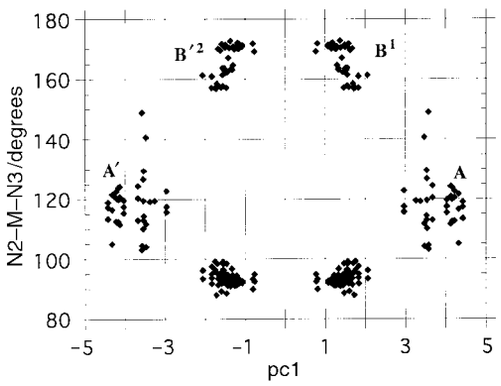

Fig. 20 Scatterplot of pc1 scores and N2–M–N3 angles (°) for $M(nn_3)$ fragments.

Fig. 21 Relation of $M(nn_3)$ δδλ and δλλ conformers (viewed down the N2–M bond) and *mer*-M(dien).

Fig. 22 δλλ and δδλ conformations of $M(nn_3)$ fragments.

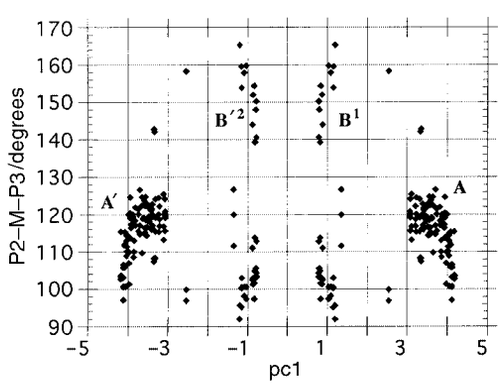

Fig. 23 Scatterplot of pc1 scores and P2–M–P3 bond angles for $M(xp_3)$ fragments.

Geometry of $M(xp_3)$ and $M(nn_3)$ fragments

The metals of $M(nn_3)$ and $M(xp_3)$ fragments show a wide variation in their coordination geometry[14,15] including tbp, octahedral, and, for $M(xp_3)$, tetrahedral (or trigonal pyramidal) and square pyramidal. Among the $M(nn_3)$ cases, all the structures in the clusters **A** and **A′** have trigonal bipyramidal coordination geometry with N2–M–N3 angles typically close to 120° (see Fig. 20), whereas fragments in clusters **B** and **B′** have octahedral geometries with one N–M–N angle in the range 155–175° (N2–M–N3 for **B**[1] and **B′**[2], see Fig. 20). It appears that the geometry at the metal affects the tripod ligand (nn_3) conformation, in rather the same way that M(dien) conformations are linked to the metal coordination geometry. Indeed, the $M(nn_3)$ fragment can be considered a derivative of M(dien) in which the hydrogen of the central nitrogen has been replaced by a third chelating arm (see Fig. 21). Thus, **A** type fragments contain a *fac*-M(dien)-like moiety with an N1–M–N3 angle *ca.* 120°, and as expected from the M(dien) study above, the two rings in these moieties have δδ (or λλ) conformations whereas the **B** or **B′** units contain *mer*-M(dien)-type moieties and therefore their two rings have δλ conformations. In each case the δ or λ conformation of the third ring (see Figs. 21 and 22) completes the {δ, λ} triplet that defines the overall conformation type of the $M(nn_3)$ unit. Of the six **B** and **B′** conformers, if the N1–M–N2 angle is >155° the conformation is of the λδδ or λδλ type; if N2–M–N3 is the large angle then δλδ or λλδ conformers result and for large N1–M–N3 δδλ and δλλ conformations are seen (see Fig. 22). This effect is then responsible for the relative proximity of these pairs of clusters in the conformation space and hence the favoured pathways for the conformer interconversion noted above. The situation for $M(xp_3)$ fragments is broadly similar, as shown in Fig. 23, in which the P2–M–P3 bond angle is plotted against pc1 scores for the $M(xp_3)$ dataset. Fragments in clusters **A** are all of trigonal bipyramidal or tetrahedral geometry whereas those in clusters **B** have one larger angle, typically between 148 and 162°. Cluster **B** structures have approximately octahedral or square pyramidal geometries at the metal. This link between ligand conformation and metal coordination geometry implies that conformer interconversion (*e.g.* stepwise from **A** to **A′** by δδδ to δλδ to λλδ to λλλ steps, see above) will proceed with concomitant variations in metal coordination geometry and in particular with changes in the P–M–P (or N–M–N) angles. Fig. 24 shows one of the three equivalent paths for interconversion of **A** and **A′** conformers.

All the $M(pp_3)$ structures in this study are tetradentate with M–X bond lengths between 2.10 and 2.30 Å, whereas 14 of the 30 $M(np_3)$ are tridentate with M · · · N distances ⩾2.5 Å. This is consistent with the M–P bond being stronger than the M–N bond in these fragments,[42] and with the greater tendency to pyramidality for the heavier pnictogen. When the ligand is tetradentate both $M(pp_3)$ and $M(np_3)$ can adopt either **A**- or **B**-type conformations [nine $M(pp_3)$ and four $M(np_3)$ fragments do so] while all of the tridentate fragments are in cluster **A** and thus have λλλ or δδδ conformations.

The more tightly clustered appearance of the scatterplots for $M(nn_3)$ as compared with $M(xp_3)$ fragments suggest that the $M(nn_3)$ fragment is less flexible than $M(xp_3)$. This also is

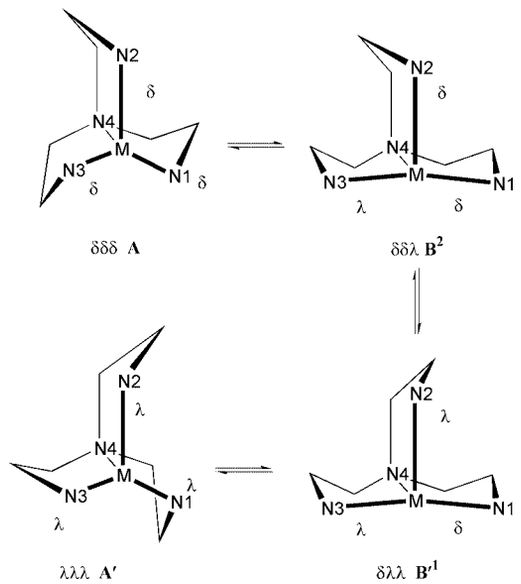

Fig. 24 Likely intermediates in one of three equivalent paths for the interconversion of **A** and **A′** conformers.

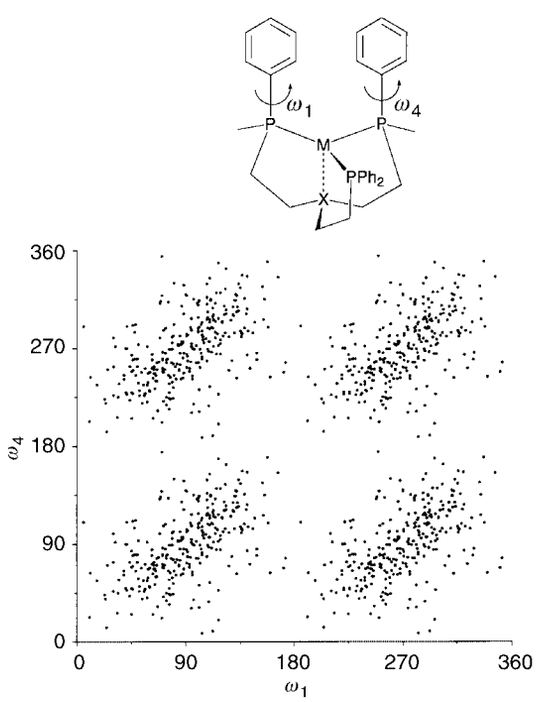

Fig. 25 Scatterplot of ω_1 and ω_4 values for $M(xp_3)$ fragments.

reflected by the limited range of N4–M bond lengths. For $M(xp_3)$ fragments the central X–M distance varies from 2.0 to 3.5 Å. In contrast, the central N4–M bond length of $M(nn_3)$ ranges only from 1.9 to 2.4 Å (with only two fragments having M–N4 > 2.2 Å). The rigidity of $M(nn_3)$ has also been observed from strain minimization calculations and molecular models.[43]

For the $M(xp_3)$ system the orientations of the six phenyl groups are strongly correlated with one another. We have previously noted the coupled rotation of two phenyls on a single phosphorus in M(dppe)[16] and $M_2(PPh_2)$[44] species. In the M(dppe) system transannular interactions between phenyl groups are so weak that almost no correlation between their orientations can be observed.[16] The increased transannular coupling of orientation notable in Fig. 25 is presumably due to the congested nature of the poly-phenylated exterior of the xp_3 ligand. The implication of this observation is that there may be opportunities to design asymmetric tripodal ligands derived from pp_3 or np_3 in which, for example, the chirality of the **A** conformer is efficiently expressed by the phenylated exterior of the ligand. Further analysis of the phenyl orientations indicates that the clustering of points in such scatterplots is dependent upon the conformer type (**A** or **B**) as might be expected given the differences in metal coordination geometries associated with the two conformers.

Conclusions

This study has analysed conformations of five-membered chelate rings in single and doubly- and triply-fused ring systems using principal component analysis. As noted above, the Altona and Sundaralingam[19] and Cremer–Pople[20] and other methods have been applied to the study of conformations of single five-membered rings on many occasions.[17,18,21] While the former method can only be used for five-membered rings and the Cremer–Pople approach can be applied to 4-, 5-, 6- and higher-membered rings, neither is used for study of fused ring systems, for which alternative approaches have been used (see refs. 45 and 46). For all the fragments analysed here PCA gives a significant reduction in the dimensionality of the conformation space, and this in turn has allowed the conformational behaviour of the fragments to be more easily identified and understood.

It can be difficult to give meaning to the principal components obtained by PCA since the linear combinations are obtained by mathematical methods without reference to the underlying characteristics of the systems under study. In this study, however, the pseudo-PC values provide a simple classification scheme which can be assigned chemical meaning. The two main components for any one five-membered ring are of twist and envelope forms. Thus the symmetric twist δ conformers have ppc(tw) ≈ 2.0 and ppc(env) = 0.0, the λ conformers ppc(tw) ≈ −2.0 and ppc(env) = 0.0; symmetric envelopes have ppc(tw) = 0.0 and ppc(env) ≈ ±2.0, whereas asymmetric envelope (*gauche*) δ conformers typically have ppc(tw) ≈ 2.0 and ppc(env) between 1.0 and 2.0 or −1.0 and −2.0; and λ conformers have ppc(tw) *ca.* −2.0. For the fused five-membered ring systems M(dien), $M(xp_3)$ and $M(nn_3)$ pseudo-PC scores show that the five-membered rings have symmetric twist or asymmetric envelope (*gauche*) conformations, and for M(dien) and $M(nn_3)$ more distorted conformations result than for the analogous single ring systems.

Among the important conclusions of the present study are the following.

(1) Ring conformations in fused-ring polychelates are efficiently analysed by principal component analysis. Conformational scatterplots in the reduced dimensional space of the PCs are readily interpreted.

(2) This analysis reveals a limited number of preferred conformers for each system: enantiomeric twist conformations (δ or λ) for M(en), M(tmeda), M(dppe) and M(dmpe); three unique conformers: δδ (or its enantiomer λλ), λδ or δλ for M(dien); and two types for $M(nn_3)$ or $M(xp_3)$: two enantiomeric C_3 symmetric **A** or six equivalent **B** conformers of low symmetry.

(3) The pathways between preferred conformers may be inferred, at least in part. Thus the pseudorotation pathway for δ/λ interconversion in the single ring systems is clear for M(dppe) and also for M(dmpe) but less so for the diamines. The fused-ring systems are more constrained and so full pathways are not clear but the sequence of δ/λ ring inversion required to interconvert conformers may be inferred. For M(dien) this involves the conversion of δλ to λδ conformers apparently through δδ (or λλ) intermediates with one ring at a time inverting. Similarly the interconversion of conformers in the $M(xp_3)$ and $M(nn_3)$ systems seems likely, on the basis of the distribution of structures in conformation space, to follow the sequence δδδ ↔ δλδ ↔ λλδ ↔ λλλ (or its equivalent) but not δδδ ↔ δλδ ↔ δλλ ↔ λλλ.

(4) The conformers preferred for M(dien), M(nn_3) and M(xp_3) systems are linked to the metal coordination geometry and in particular the presence (or not) of a P–M–P or N–M–N angle approaching 180°. This observation, taken with that above, implies that conformer interconversions take place concomitantly with changes in the N–M–N (or P–M–P) bond angles from *ca.* 180° to *ca.* 90° (or *vice versa*) as the dien (or nn_3 or xp_3) ligand coordination mode adjusts (*e.g.* from *mer* to *fac* in the case of dien).

(5) The M–N (M–P) bond length is correlated with the ring conformations in these species such that long M–N (or M–P) distances enforce more puckered, symmetrical, twist conformations of five-membered rings.

(6) Use of the new pseudo-principal component analysis method facilitates quantitative comparison of conformations in analogous but not identical ring systems. Its use reveals the differing degrees of ring conformation puckering in, for example, M(en) compared with M(dien) or M(nn_3).

(7) The phosphine systems exhibit greater variation of conformation than their amine counterparts. In particular, M(dmpe) systems show considerably more variation than M(tmeda). Similarly, the effect of substituents at the phosphorus is apparent in that M(dppe) species are more varied in conformation than are M(dmpe). Apparently the effect of the larger substituents at phosphorus is to leverage the distortions in the chelate rings.

Finally it is worth noting that these observations on the geometry and conformation of metal polyphosphine and amine complexes may help to develop ligand design through understanding of the conformational preferences of such systems, their flexibility and the factors which select one conformer over another.

Acknowledgements

We thank the many chemists and crystallographers who synthesized the compounds and determined the structures discussed in this paper. We thank the EPSRC for a Research Studentship (S. E. H.) and the EU for a TMR Fellowship (I. P.).

References

1 Part 8. M. J. Quayle and A. G. Orpen, *J. Chem. Soc., Dalton Trans.*, 2001, 1601.
2 E. J. Corey and J. C. Bailar, *J. Am. Chem. Soc.*, 1959, **81**, 2620.
3 (*a*) J. R. Gollogly and C. J. Hawkins, *Inorg. Chem.*, 1969, **8**, 1168; (*b*) J. R. Gollogly and C. J. Hawkins, *Inorg. Chem.*, 1970, **9**, 576; (*c*) J. R. Gollogly, C. J. Hawkins and J. K. Beattie, *Inorg. Chem.*, 1971, **10**, 317; (*d*) J. R. Gollogly and C. J. Hawkins, *Inorg. Chem.*, 1972, **11**, 156.
4 G. R. Brubaker and D. W. Johnson, *Coord. Chem. Rev.*, 1984, **53**, 1.
5 L. J. DeHayes and D. H. Busch, *Inorg. Chem.*, 1973, **12**, 1505.
6 C. J. Hawkins and J. A. Palmer, *Coord. Chem. Rev.*, 1982, **44**, 1.
7 J. K. Beattie, *Acc. Chem. Res.*, 1971, **4**, 253.
8 Y. Kuroda, N. Tanaka, M. Goto and T. Sakai, *Inorg. Chem.*, 1989, **28**, 997.
9 T. W. Hambley, *J. Comput. Chem.*, 1987, **8**, 651.
10 Z. J. Guo, A. Habtemariam, P. J. Sadler, R. Palmer and B. S. Potter, *New J. Chem.*, 1998, **22**, 11.
11 *Comprehensive Coordination Chemistry*, ed. G. Wilkinson, J. A. McCleverty and R. D. Gillard, Pergamon Press, Oxford, 1987, vol. 2.
12 (*a*) C. Bianchini, D. Masi, C. Mealli and A. Meli, *Inorg. Chem.*, 1984, **23**, 2838; (*b*) P. Dapporto, S. Midollini, A. Orlandini and L. Sacconi, *Inorg. Chem.*, 1976, **15**, 2768; (*c*) C. Bianchini, D. Masi, A. Meli, M. Peruzzini and F. Zanobini, *J. Am. Chem. Soc.*, 1988, **110**, 6411.
13 (*a*) C. Bianchini, A. Meli and A. Orlandini, *Inorg. Chem.*, 1982, **21**, 4166; (*b*) M. Di Vaira, B. E. Mann, M. Peruzzini and P. Stoppioni, *Inorg. Chem.*, 1988, **27**, 3725; (*c*) C. Bianchini, C. Mealli, A. Meli and L. Sacconi, *Inorg. Chim. Acta*, 1979, **37**, L543.
14 (*a*) C. A. Ghilardi, C. Mealli, S. Midollini and A. Orlandini, *Inorg. Chem.*, 1985, **24**, 165; (*b*) C. A. Ghilardi, S. Midollini, S. Moneti, A. Orlandini, G. Scapacci and A. Traversi, *J. Chem. Soc., Dalton Trans.*, 1990, 2293; (*c*) C. A. Ghilardi, C. Mealli, S. Midollini, A. Orlandini, D. M. Proserpio, A. Cinquantini and P. Zanello, *Struct. Chem.*, 1990, **1**, 441.
15 C. Mealli, C. A. Ghilardi and A. Orlandini, *Coord. Chem. Rev.*, 1992, **120**, 361.
16 D. A. V. Morton and A. G. Orpen, *J. Chem. Soc., Dalton Trans.*, 1992, 641.
17 F. H. Allen, M. J. Doyle and T. P. E. Auf der Heyde, *Acta Crystallogr., Sect. B*, 1991, **47**, 412.
18 F. H. Allen, P. R. Raithby and G. P. Shields, *Struct. Chem.*, 1997, **8**, 385; P. R. Raithby, G. P. Shields and F. H. Allen, *Acta Crystallogr., Sect. B*, 1997, **53**, 241.
19 C. Altona and M. Sundaralingam, *J. Am. Chem. Soc.*, 1972, **94**, 8205.
20 D. Cremer and J. A. Pople, *J. Am. Chem. Soc.*, 1975, **97**, 1354.
21 (*a*) F. H. Allen, M. J. Doyle and R. Taylor, *Acta Crystallogr., Sect. B*, 1991, **47**, 29; (*b*) F. H. Allen, M. J. Doyle and R. Taylor, *Acta Crystallogr., Sect. B*, 1991, **47**, 41; (*c*) F. H. Allen, M. J. Doyle and R. Taylor, *Acta Crystallogr., Sect. B*, 1991, **47**, 50; (*d*) C. A. G. Haasnoot, *J. Am. Chem. Soc.*, 1992, **114**, 882.
22 C. Chatfield and A. J. Collins, *Introduction to Multivariate Analysis*, Chapman and Hall, London, 1980.
23 J. D. Dunitz, *X-Ray Structure Analysis and the Structure of Organic Molecules*, Cornell University Press, Ithaca, NY, 1979.
24 A. G. Orpen, *Chem. Soc. Rev.*, 1993, 191.
25 V. Rodriguez, J. M. Gutierrez-Zorrilla, P. Vitoria, A. Luque, P. Roman and M. Martinez-Ripoll, *Inorg. Chim. Acta*, 1999, **290**, 57.
26 F. H. Allen and O. Kennard, *Chem. Des. Automat. News*, 1993, **8**, 1; F. H. Allen and O. Kennard, *Chem. Des. Automat. News*, 1993, **8**, 31.
27 F. H. Allen, J. E. Davies, J. J. Galloy, O. Johnson, O. Kennard, C. F. Macrae, E. M. Mitchell, G. F. Mitchell, J. M. Smith and D. G. Watson, *J. Chem. Inf. Comput. Sci.*, 1991, **31**, 187.
28 SYSTAT Inc., version 5.2, Evanston, IL.
29 A. G. Orpen, L. Brammer, F. H. Allen, O. Kennard, D. G. Watson and R. Taylor, *J. Chem. Soc., Dalton Trans.*, 1989, S1; A. Martín and A. G. Orpen, *J. Am. Chem. Soc.*, 1996, **118**, 1464.
30 *Structure Correlation*, ed. H.-B. Bürgi and J. D. Dunitz, Verlag Chemie, Weinheim, 1994.
31 H. C. Longuet-Higgins, *Mol. Phys.*, 1963, **6**, 445.
32 P. Murray-Rust and S. Motherwell, *Acta Crystallogr., Sect. B*, 1978, **34**, 2534.
33 J. E. Kilpatrick, K. S. Pitzer and R. Spitzer, *J. Am. Chem. Soc.*, 1947, **69**, 2483.
34 F. Pavelcík and E. Luptáková, *Collect. Czech. Chem. Commun.*, 1990, **55**, 1427.
35 M. C. Hall, B. T. Kilbourn and K. A. Taylor, *J. Chem. Soc. A*, 1970, 2539.
36 S. Siegel, *Non-Parametric Statistics*, McGraw-Hill, New York, 1956.
37 C. J. Hawkins, R. M. Peachey and C. L. Szoredi, *Aust. J. Chem.*, 1978, **31**, 973.
38 H. H. Schmidtke and D. Garthoff, *Inorg. Chim. Acta*, 1968, **2**, 357.
39 A. M. Bond, T. W. Hambley and M. R. Snow, *Inorg. Chem.*, 1985, **24**, 1920.
40 (*a*) J. F. Britten and C. J. L. Lock, *Acta Crystallogr., Sect. B*, 1980, **36**, 2958; (*b*) J. F. Britten, C. J. L. Lock and W. M. C. Pratt, *Acta Crystallogr., Sect. B*, 1982, **38**, 2148.
41 W. G. Jackson, A. M. Sargeson, P. A. Tucker and A. D. Watson, *J. Am. Chem. Soc.*, 1981, **103**, 533.
42 F. Cecconi, C. A. Ghilardi, P. Innocenti, C. Mealli, S. Midollini and A. Orlandini, *Inorg. Chem.*, 1984, **23**, 922.
43 Y. Mitsui, J. Watanabe, Y. Harada, T. Sakamaki, Y. Iitaka, Y. Kushi and E. Kimura, *J. Chem. Soc., Dalton Trans.*, 1976, 2095.
44 J. J. Barker and A. G. Orpen, *Acta Crystallogr., Sect. B*, 1999, **55**, 203.
45 S. Beyreuthe, J. Hunger, G. Huttner, S. Mann and L. Zsolnai, *Chem. Ber.*, 1996, **129**, 745.
46 M. A. Donnelly and M. Zimmer, *Inorg. Chem.*, 1999, **38**, 1650.